Nanoscale

PAPER

View Article Online
View Journal | View Issue

Cite this: *Nanoscale*, 2022, **14**, 5147

DNA/RNA sequencing using germanene nanoribbons *via* two dimensional molecular electronic spectroscopy: an *ab initio* study†

M. Reza Rezapour * and Blanca Biel

Received 5th November 2021,
Accepted 28th February 2022

DOI: 10.1039/d1nr07336b

rsc.li/nanoscale

Developing fast, reliable, and cost effective, yet practical DNA/RNA sequencing methods and devices is a must. In this regard, motivated by the recently introduced two-dimensional electronic molecular spectroscopy (2DMES) technique for molecular recognition, and the compatibility of 2D layers of group IV elements with the current technology of manufacturing electronic devices, we investigate the capability of germanene nanoribbons (GeNRs) as a feasible, accurate, and ultra-fast sequencing device under the application of 2DMES. We show that by employing 2DMES, not only can GeNRs unambiguously distinguish different nucleobases to sequence DNA/RNA, they are also capable of recognizing methylated nucleobases that could be related to cancerous cell growth. Our calculations indicate that, compared to frequently used graphene layers, germanene provides more distinct adsorption energies for different nucleobases which implies its better ability to recognize various molecules unambiguously. By calculating the conductance sensitivity of the system for experimental purposes, we also show that the introduced sequencing device possesses a high sensitivity and selectivity characteristic. Thus, our proposed system would be a promising device for next-generation DNA sequencing technologies and would be realizable using the current protocols of fabricating electronic devices.

Introduction

2D materials have progressed rapidly across a diversity of scientific and engineering subfields, including next-generation nanoelectronics, owing to their fascinating electrical, optical, chemical, thermal, and structural properties.[1–7] Among the 2D materials, graphene has been the epitome of all such materials.[8,9] Graphene and graphene nanoribbons have diverse applications in various sectors from electronics to energy, to health and to the environment.[10–25] The wide application range of graphene has motivated experimental research to explore other 2D compounds, such as hexagonal boron-nitride,[26,27] silicene,[28,29] germanene,[30] stanene,[31] phosphorene,[32,33] and transition metal dichalcogenides,[34,35] Among graphene-analogue 2D monolayers, those composed of group IV elements such as silicene[36–38] and germanene[39–41] are of particular interest due to their full adaptability with the currently in-use protocols of device fabrication and integration in the present silicon and germanium based semiconductor technologies. They also show excellent flexibility and compressibility relative to graphene, while strain engineering has been proposed to modify their electronic and thermal properties. Such aspects make these materials an acceptable candidate for creating nano-electromechanical systems and sensors that can integrate well with the current generation of device technology.[42] In line with the efforts for the practical exploitation of these 2D materials, hydrogen-terminated germanene was synthesized by adding covalently bonded hydrogen on both sides of germanene.[43] Recently, Chen *et al.* showed that thermally annealed germanene has structural stability at room temperature and exhibits a highly conductive metallic state.[44] However, for nanoelectronics applications, the material requirement is to be semiconductive and with a tunable band gap. Since the quantum confinement is a known technique for band gap modulation, GeNR in both armchair GeNR (AGeNRs) and zigzag GeNR (ZGeNR) forms were studied.[44] It was shown that the band gap of AGeNR varies in an oscillatory motion by increasing its width, whereas ZGeNR shows a ferromagnetic behavior along its edges.[45,46]

It should be noted that the crystal structure of germanene does not exactly resemble that of graphene, as it exhibits a buckled honeycomb structure instead of the flat honeycomb phase of graphene.[41,47] Intriguingly, unlike carbon atoms in graphene, in germanene, germanium atoms tend to adopt sp^3 hybridization over sp^2, which makes it highly chemically active on the surface and hence promising for applications such as

Department of Atomic, Molecular and Nuclear Physics, Faculty of Science, Campus de Fuente Nueva, University of Granada, 18071 Granada, Spain.
E-mail: rezapour@ugr.es

†Electronic supplementary information (ESI) available. See DOI: 10.1039/d1nr07336b

batteries,[48] catalysts,[49] and sensors.[50] This feature also allows the electronic states of germanene to be easily tuned by chemical functionalization[51] such as adsorption,[52,53] which is an important approach for molecular sensing and DNA sequencing.[54] It is worth mentioning that although the interaction of various gas molecules with germanene monolayers has been extensively studied,[55–57] its interaction with biomolecules such as DNA/RNA nucleobases has only been very limitedly investigated.

A pioneer study on the application of group IV elemental monolayers as potential biosensors has been conducted by Amorim and Scheicher,[58] who comprehensively investigated silicene as a promising building block of a DNA sequencing device. Later, Hussain, *et al.* also studied the adsorption characteristics of DNA nucleobases, aromatic amino acids and heterocyclic molecules on 2D silicene and germanene monolayers.[59] On the other hand, the technique called two dimensional molecular electronic spectroscopy (2DMES), introduced in our previous works,[60] has been shown to be efficient in unambiguously recognizing and distinguishing various molecules including DNA/RNA bases and their mutated forms. In this technique, once a molecule is adsorbed onto a monolayer, the relative differential conductance (Δg with respect to the differential conductance of the pristine monolayer) of the molecule–monolayer system is mapped with respect to bias and gate voltages. The observed dips in the electron transmission spectrum of the complex, which emerged due to the Fano resonance,[61] are shown to be unique electronic fingerprints of the adsorbed molecule and thus can be utilized for molecular sensing and DNA/RNA sequencing.

Motivated by all these findings, in this work, we investigate the capability of AGeNR as a nano-biosensor for DNA/RNA sequencing under the application of the 2DMES technique. For this purpose, first, we briefly study the structural and electronic characteristics of AGeNRs. Next, the adsorption of various nucleobases onto AGeNR and the thermodynamic stability of the obtained nucleobases–AGeNR complexes are examined. The selected nucleobases are adenine (A), cytosine (C), guanine (G), thymine (T), uracil, 5-methylcytosine (5mC), and 5-hydroxymethylcytosine (5hmC), in which the latter two were selected because of their potential role in cancer cell growth. In the following step, we calculate transmission profiles of the introduced nucleobase–AGeNR systems and show that once a DNA/RNA base is adsorbed onto the AGeNR's surface, the ballistic electron transfer mode exhibits a new path with dips at certain energies. To investigate the possibility of uniquely assigning the emerged Fano dips as molecular fingerprints to each nucleobase in an AGeNR based sequencing device, we calculate and plot Δg spectra for each nucleobase–AGeNR system for a certain range of bias and gate voltages. Comparing the obtained 2D and three-dimensional (3D) Δg maps indicates that AGeNR can be employed to unambiguously recognize and distinguish various nucleobases provided 2DMES is applied. By calculating the conductance sensitivity, we also show that AGeNR is able to recognize various nucleobases with acceptable sensitivity.

Computational methods

Our first-principles calculations are performed based on density functional theory (DFT). The Vienna *ab initio* simulation package (VASP)[62] is used to optimize all the geometries and investigate the electronic structures of the systems. To treat the exchange–correlation effects, we employ the generalized gradient approximation (GGA) of Perdew, Burke, and Ernzerhof (PBE).[63] The plane-augmented wave (PAW) method is used to describe the electron–ion interactions and the Kohn and Sham orbitals are expanded in a plane wave basis set.[64]

Since the nucleobase–AGeNR interaction in the proposed system is governed by van der Waals (vdW) forces,[65,66] we also include a functional accounting for dispersion effects, representing these forces in accordance with the method developed by Tkatchenko–Scheffler (TS),[67] which is implemented on VASP.[68]

The cutoff energy for the grid-mesh is 500 Ry in the calculations and a k-point mesh of $1 \times 1 \times 64$ is employed along the x, y, and z directions, respectively. All the structures are fully relaxed until energy and forces are converged to 10^{-5} eV and 0.01 eV Å^{-1}, respectively. To investigate the transport characteristics of the systems, DFT combined with nonequilibrium Green's function (NEGF),[69,70] as implemented in TranSIESTA,[71] is utilized. The transmission is given by:

$$T_\sigma(E, V_b) = \mathrm{Tr}[\Gamma_L G \Gamma_R G^\dagger] \quad (1)$$

where Tr stands for the trace, $\Gamma_{L/R} = i[\Sigma_{L/R} - \Sigma_{L/R}^\dagger]$ with $\Sigma_{L/R}$ as the self-energy of the left/right electrode, and $G = [E - H - \Sigma_L - \Sigma_R]^{-1}$ denotes Green's function with the scattering region Hamiltonian H. On the basis of Landauer–Büttiker formalism, the source–drain current is:

$$I(V_b) = \frac{2e}{h}\int T(E, V_b)[f(E, \mu_L) - f(E, \mu_R)]\mathrm{d}E \quad (2)$$

where $f(E,\mu_L)$ is the Fermi–Dirac function with the associated chemical potential of $\mu_{L/R} = E \pm \frac{V_b}{2}$, which is a shifted value relative to the Fermi level of neutral system E_F.

Results and discussion

Atomic and electronic structure

To perform the study, we chose an 8-AGeNR, in which 8 stands for the number of dimer lines along the width of the AGeNR. For simplicity, from now on 8-AGeNR will be denoted as AGeNR unless otherwise specified. The dangling bonds on the edges of AGeNR are hydrogen-terminated. Fig. 1a and b show the front and side views of the chosen AGeNR schematically, in which the lattice constant, a, in similarity with 2D germanene, the buckling height, b, and the primitive unit cell (dashed-lines rectangle) with cell length c, are specified. The thermodynamic stability of germanene nanoribbons has already been discussed in the literature, where it has been shown that the low buckled form of germanene is energetically more favorable and behaves as a semi-metal.[72–74] Our calcu-

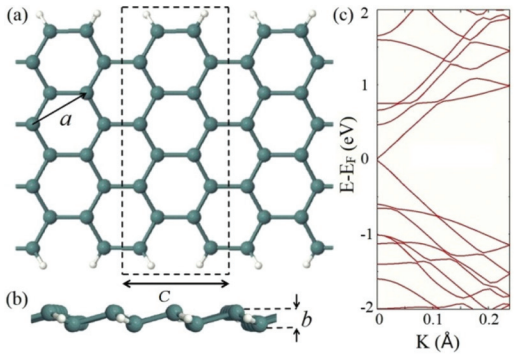

Fig. 1 Schematic illustration of (a) the front and (b) the side view of AGeNR. The lattice constant, the buckling height, and the primitive unit cell (the black dashed line box) length are represented by *a*, *b*, and *c*, respectively. (c) The band structure of AGeNR.

lated values for *a*, *b*, and *c* are 3.96 Å, 0.64 Å, and 6.96 Å, respectively, in agreement with previous studies.[44,72] Fig. 1c depicts the calculated band structure of AGeNR. The plotted energy band diagram represents the semi-metal nature of the system with a band gap of 0.036 eV, in agreement with the band gap behavior of low buckled AGeNRs with a width of the group $3p + 2$ (p is an integer number).[44,46]

Adsorption configurations

Initially, each nucleobase is deposited at the middle of the AGeNR, on different adsorption sites with different orientations, yet parallel to the AGeNR surface at a distance of 3 Å. Here, we follow the results on the adsorption behavior of nucleobases on germanene obtained from previous studies.[59,74] The separation distance is defined between nucleobase and AGeNR (d) as the distance between the nearest atoms of the two subsystems. Although the initial positions and orientations of the nucleobase are arbitrarily chosen, however, since the interaction between the nucleobase and the substrate is mediated by weak vdW forces,[75] the variation of adsorption energy for different nucleobase–AGeNR configurations would be negligible.[76] Fig. 2 shows the fully relaxed configurations of the studied nucleobase–AGeNR complexes. It is inferred from Fig. 2 that except for adenine, which is stacked on AGeNR in parallel, other nucleobases take tilted orientations towards the AGeNR surface. It is also noteworthy that, unlike the adsorption of nucleobases on silicene, in which C and G chemically bond with the substrate (a process of an exothermic nature),[58] here all the bases exhibit physisorption interaction with the AGeNR, which might be due to the endothermic nature of dissociative adsorption of some oxygen containing molecules on the germanene surface.[77]

To investigate the relative stability of nucleobases on top of the AGeNR surface, we calculate the adsorption energy (E_{ad}) using the following equation:

$$E_{ad} = E_{AGeNR+nb} - (E_{AGeNR} + E_{nb}) \quad (3)$$

where $E_{AGeNR+nb}$, E_{AGeNR}, and E_{nb} are the total energies of the optimized nucleobase–AGeNR system, pristine AGeNR, and

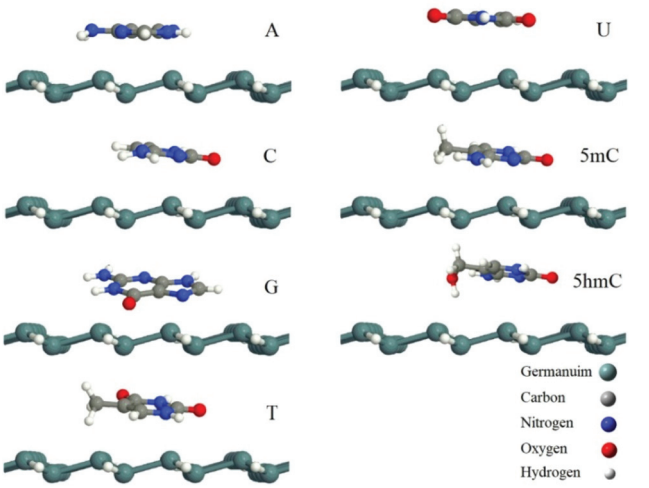

Fig. 2 Optimized structures of the studied nucleobase–AGeNR systems. The color key of the atoms is illustrated in the bottom right panel.

the isolated nucleobase respectively. Table 1 summarizes the calculated E_{ad} and optimized d values for the studied nucleobase–AGeNR systems. It can be seen from Table 1 that the order of the adsorbed nucleobases onto the AGeNR in terms of E_{ad} is G > A > T > C > 5mC > 5hmC > U which is in agreement with previous studies.[59] As a comparison, it is worth noting that the nucleobases present the order G > A ≈ T ≈ C > U in terms of E_{ad} when adsorbed onto graphene.[78] This larger separation of the adsorption energies points towards the better suitability of germanene over graphene for unambiguous recognition of nucleobases. Based on these calculated E_{ad} values, it can be seen that the interaction with the AGeNR is determined by its distance to the AGeNR and increases with decreasing d: G, with the smallest d, strongly interacts with the AGeNR, while U, with the largest d, has the weakest interaction. The magnitude of E_{ad} and d values also indicates the vdW nature of the interaction between nucleobases and AGeNR. It should be noted that, since E_{ad} in a nucleobase–AGeNR system represents the magnitude of the coupling parameter in the Fano–Anderson model,[61,79] different E_{ad} values imply that nucleobases can be distinguished unambiguously *via* Fano resonance driven 2DMES.

In order to further investigate the adsorption of nucleobases on AGeNR and the nature of the interaction between two segments of the system, we calculate and plot the charge density redistribution of the studied nucleobase–AGeNR com-

Table 1 Adsorption energies (E_{ad}) of nucleobases onto the AGeNR's surface and the separation distance (d) between different nucleobases and AGeNR

	A	C	G	T	U	5mC	5hmC
E_{ad} (eV)	−0.73	−0.58	−0.85	−0.61	−0.50	−0.55	−0.54
d (Å)	2.98	3.05	2.76	3.02	3.11	3.05	3.06

plexes as depicted in Fig. S1 in the ESI.† It can be seen from the plotted isosurfaces that, in all the studied nucleobase–AGeNR systems, the final charge density is concentrated mainly on the nucleobase and there is no complex charge density redistribution between nucleobases and AGeNR. This clearly indicates that the interaction between the two parts of the system is ruled by weak and purely non-covalent forces which confirms the adsorption nature of the nucleobases onto the AGeNR's surface to be physisorption.

Charge transport properties

On the basis of the above analyses, we calculate the charge transport properties for all the introduced nucleobase–AGeNR structures along the AGeNR's axis direction. Fig. 3a illustrates a schematic representation of the proposed two-probe transport configuration, which can be modeled as a Fano–Anderson chain. Thus, peaks/dips in the transmission profile of each nucleobase–AGeNR system due to the Fano effect can be expected. Fig. 3b shows the calculated transmission profiles of the studied nucleobase–AGeNR structures as well as the bare AGeNRs at zero bias voltage (V_b).

It is followed from Fig. 3b that the adsorption of a nucleobase onto the AGeNR surface results in sharp reductions in the transmission spectrum of AGeNR at certain energies that can be controlled by the application of gate voltage (V_g). Since the transport characteristics of a nucleobase attached on the AGeNR surface strongly depend on the frontier molecular orbital (MO) energy levels, the emerged dips in the transmission profile can be assigned to each molecule uniquely and hence utilized for recognition and sequencing purposes. This is confirmed by investigating the projected density of states (PDOS) of the nucleobase–AGeNR systems, as shown in the inset of Fig. 3b, which is plotted with respect to the DOS of pristine AGeNR. As shown in the plotted PDOS profiles, adsorbed molecules induce strong states to the electronic structure of AGeNR in the energy values consistent with the energy values of the emerged transmission reductions. One can see that except for uracil, the other nucleobases provide at least one energetically distinct transmission reduction, and hence distinguishable from those of the other nucleobases. Fig. 3b shows that the four canonical bases of A, C, G, and T, once adsorbed on the AGeNR, provide Fano dips at $E - E_F$ = −0.42 (as well as −0.70), −0.98, −0.46 (as well as −1.84) and −1.07 eV, respectively, which makes these bases unambiguously distinguishable. In the case that methylated C derivatives *i.e.* 5mC and 5hmC are attached to the AGeNR's surface, transmission reductions arise at $E - E_F$ = −1.03, −0.95 eV respectively. For the case of U adsorbed on the AGeNR, a transmission reduction appears at $E - E_F$ = −1.03 eV, whose emerged Fano dip is minor compared to those of the other studied systems due to the lower E_{ad} of U and the larger d. Besides, the molecular fingerprint of U is situated within the energy range of the transmission reductions of C, 5mC, and T which prevents unambiguous discrimination of U. However, in the following we show that although molecular fingerprints of some nucleobases are energetically adjacent, they can be recognized and distinguished without any ambiguity by employing the 2DMES technique.

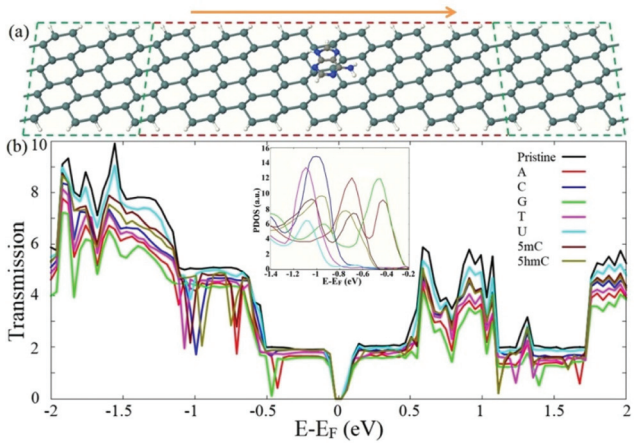

Fig. 3 (a) Schematic illustrations of the proposed two-probe transport system composed of an AGeNR with a nucleobase adsorbed onto its surface. The left and right electrodes are indicated by the green dashed line boxes, while the red dashed lines define the scattering region. The arrow represents the transport direction (b) transmission profiles of the pristine AGeNR and the studied nucleobase–AGeNRs structures at zero V_b. The inset represents the PDOS of nucleobase–AGeNR systems with respect to DOS of pristine AGeNR.

Application of 2DMES

In practice, it is the conductance of a biosensor that is measured. Thus, we calculate Δg of the proposed sensing system at varying V_b and V_g ($E - E_F$ equally). It is also worth noting that since the 1D-conductance changes by a unit of quantum conductance, measuring it rather than the current provides more accurate distinction of the variation of the biosensor's signal. The 2D and 3-dimensional (3D) views of the calculated Δg ($-\Delta g$ for visual aids) with respect to V_b and V_g for different nucleobase–AGeNR systems are depicted in Fig. 4. The illustrated plots explicitly represent distinct features of Δg graphs for various studied systems where the variation of the Δg surface for each system is different. It means that, even in the case of two nucleobases providing Fano dips at contiguous energies, their Δg maps in the vicinity of their molecular fingerprints would still be different, which enables their unambiguous recognition and distinction. From the experimental view, it is noteworthy that the required time for measurements is the number of the selected bias voltages times the time for a gate voltage sweep. However, not many bias voltages are necessary to distinguish nucleobases; only measurements at two or three different bias voltages would be sufficient. Therefore, the time required for a reliable measurement is of a similar order of magnitude to the case when the bias voltage is not controlled. On the other hand, as it can be seen from Fig. 4, sweeping electron transport channels in an energy range of 1 eV would be enough to provide a Δg map for each nucleobase that includes its unique and distinct electronic fingerprints. This is in contrast to the 1D plot of the transmission

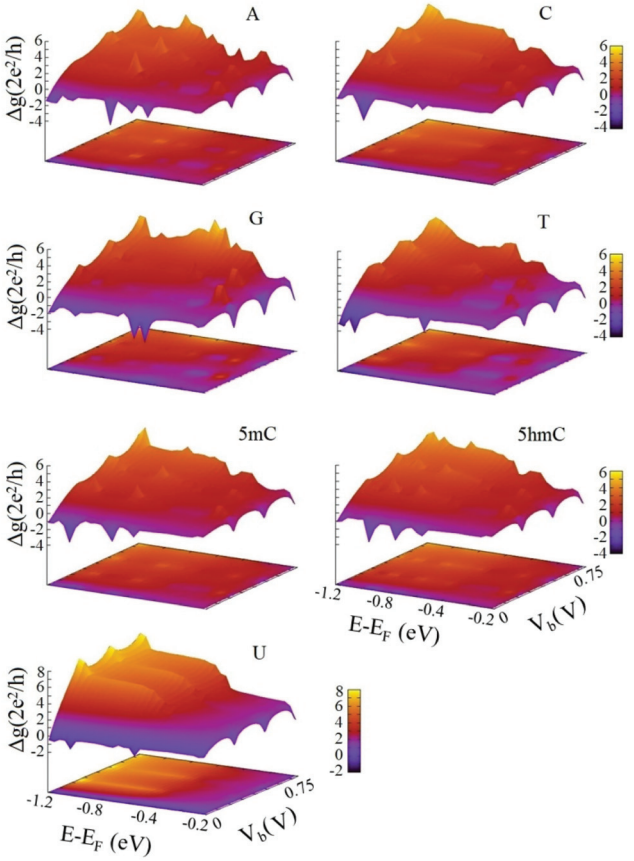

Fig. 4 2D and 3D maps of differential conductance, Δg, for different nucleobase–AGeNR systems with respect to electron channel energies ($E - E_F$) at varying bias voltages V_b.

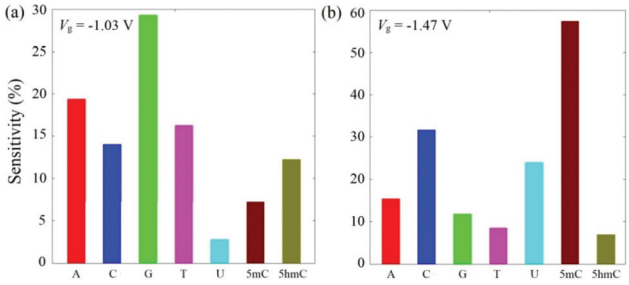

Fig. 5 Sensitivity histograms of AGeNR for different nucleobases at (a) V_g = −1.03 V and (b) V_g = −1.47 V.

spectrum (or eventually the current–voltage graphs as shown in Fig. S3 in ESI†) which might be unable to distinctly recognize different nucleobases due to the overlap of their corresponding molecular fingerprints. This is the reason why the 2DMES technique can clearly recognize the molecular fingerprints, while the 1D current measurement can hardly provide accurate information on sensing molecules. For practical use, variations of Δg spectral maps for various nucleobases can be stored in a database. Then, through data search and analysis, the characterization of a molecule would be possible using the obtained Δg spectroscopy data.

To provide further insight on the susceptibility of the introduced sequencing method in recognizing different nucleobases, we also calculate the conductance sensitivity (S) of the proposed system. In general, S can be defined as $S(\%) = |g - g_0|/g_0$ where g and g_0 are the zero-bias conductance of a biosensor with and without the adsorbed molecule, respectively. Fig. 5 illustrates the calculated sensitivity for all the studied nucleobase–AGeNR systems at two different V_g values. The plotted histograms in Fig. 5 show that, in practice, the introduced germanene based sequencing device possesses the capability of recognizing different nucleobases distinctly using the measured conductance data at various corresponding V_g values. For instance, at V_g = −1.03 V, the proposed biosensor would exhibit larger sensitivities for G and A with $S(\%)$ = 29.8% and 19.3%, respectively, where the order of nucleobases in terms of the sensitivity of the device is G > A > T > C > 5mC > 5hmC > U. However, at V_g = −1.47 V, 5mC and C with $S(\%)$ = 57.3% and 31.7%, respectively, provide higher sensitivity where the order of nucleobases is as 5mC > C > U > A > G > T > 5hmC. Therefore, by sweeping V_g in a certain range, the proposed biosensor can recognize and distinguish various nucleobases despite their different interaction strength with AGeNR.

Conclusions

In summary, we studied the molecular sensing and DNA/RNA sequencing properties of armchair type germanene nanoribbon by employing the 2DMES technique. Towards this goal, we first investigated the adsorption behaviors of canonical DNA/RNA bases as well as the methylated forms of cytosine on an AGeNR. Our calculations show that the order of nucleobases in terms of their adsorption energies onto the AGeNR's surface is G > A > T > C > 5mC > 5hmC > U which exhibits more distinct adsorption energies than graphene with G > A ≈ T ≈ C > U. Then, we showed that once a nucleobase is attached onto an AGeNR, electronic fingerprints of the adsorbed base in the form of Fano dips emerge in the transmission spectrum of the nucleobase–AGeNR structure, a feature that can be utilized to recognize and distinguish the adsorbed base. In order to avoid ambiguity in recognizing various bases and also supply a feasible method to perform the required practical measurements, we employ the 2DMES technique to provide Δg spectra of the introduced complexes with respect to V_b and V_g. The calculated 2D and 3D Δg maps for different studied systems, in contrast with 1D current–voltage profiles, exhibit explicitly distinct features which enable unambiguous recognition of nucleobases. This means that, in practice, providing the Δg spectrum for each nucleobase while the nucleobase is translocating the width of AGeNR can be utilized for unambiguous molecular recognition. The provided Δg maps for various nucleobases can be stored in a data set for DNA/RNA sequencing purpose. Also, in order to demonstrate the admissible susceptibility of AGeNR to recognize various bases, we

calculate the conductance sensitivity of the proposed system and show that AGeNR can provide large sensitivities for different nucleobases at different V_g values, making it applicable for molecular sensing usages. Under the practical conditions, where the aqueous environment is present, it is expected that water molecules will affect the transport characteristics of a nano-biosensor. However, it has been shown that germanene is hydrophobic.[80] Therefore, similarly to graphene, we expect that interaction between a nucleobase and the AGeNR would be stronger than that existing between the water molecules and the AGeNR. Hence, the stacking structures would not be significantly influenced by solvent effects. However, a QM/MM study (which is beyond the scope of this manuscript) would better elucidate the solvent effect. Given that germanene is compatible with current technology of fabricating electronic devices, our proposed device in combination with the 2DMES technique can be a promising feasible nanobiosensor for DNA/RNA sequencing and cancerous DNA recognition as well as molecular sensing.

Conflicts of interest

There are no conflicts to declare.

Acknowledgements

MRR is funded by H2020 Marie Skłodowska-Curie Actions, 841673. Financial supports from AEI and FEDER under project MAT2017-88258-R (AEI/FEDER, UE) and from the Programa Operativo FEDER of Andalucía 2014-2020 under project B-FQM-272-UGR20 are gratefully acknowledged by BB. MRR gratefully acknowledges Prof. Geunsik Lee from the Ulsan National Institute of Science and Technology (UNIST) for providing computational resources of UNIST Supercomputing center. Red Española de Supercomputación (RES) and the Alhambra supercomputer of the University of Granada are also acknowledged for providing computational time and facilities.

References

1 M. Zeng, Y. Xiao, J. Liu, K. Yang and L. Fu, *Chem. Rev.*, 2018, **118**, 6236–6296.
2 K. Khan, A. K. Tareen, M. Aslam, R. Wang, Y. Zhang, A. Mahmood, Z. Ouyang, H. Zhang and Z. Guo, *J. Mater. Chem. C*, 2020, **8**, 387–440.
3 D. Akinwande, C. Huyghebaert, C. H. Wang, M. I. Serna, S. Goossens, L. J. Li, H. S. Philip Wong and F. H. L. Koppens, *Nature*, 2019, **573**, 507–518.
4 C. Liu, H. Chen, S. Wang, Q. Liu, Y. G. Jiang, D. W. Zhang, M. Liu and P. Zhou, *Nat. Nanotechnol.*, 2020, **15**, 545–557.
5 A. Cresti, N. Nemec, B. Biel, G. Niebler, F. Triozon, G. Cuniberti and S. Roche, *Nano Res.*, 2008, **1**, 361–394.
6 B. Biel, X. Blase, F. Triozon and S. Roche, *Phys. Rev. Lett.*, 2009, **102**, 096803.
7 A. Lherbier, B. Biel, Y. M. Niquet and S. Roche, *Phys. Rev. Lett.*, 2008, **100**, 036803.
8 M. J. Allen, V. C. Tung and R. B. Kaner, *Chem. Rev.*, 2010, **110**(1), 132–145.
9 M. R. Rezapour, C. W. Myung, J. Yun, A. Ghassami, N. Li, S. U. Yu, A. Hajibabaei, Y. Park and K. S. Kim, *ACS Appl. Mater. Interfaces*, 2017, **9**, 24393–24406.
10 A. C. Ferrari, *et al.*, *Nanoscale*, 2015, **7**, 4598–4810.
11 Z. H. Pan, N. Liu, L. Fu and Z. F. Liu, *J. Am. Chem. Soc.*, 2011, **133**, 17578–17581.
12 S. Thomas, A. C. Rajan, M. R. Rezapour and K. S. Kim, *J. Phys. Chem. C*, 2014, **118**(20), 10855–10858.
13 G. T. Feliciano, C. Sanz-Navarro, M. D. Coutinho-Neto, P. Ordejón, R. H. Scheicher and A. R. Rocha, *Phys. Rev. Appl.*, 2015, **3**, 034003.
14 F. Muñoz-Rojas, J. Fernández-Rossier and J. J. Palacios, *Phys. Rev. Lett.*, 2009, **102**, 136810.
15 M. R. Rezapour, J. Yun, G. Lee and K. S. Kim, *J. Phys. Chem. Lett.*, 2016, **7**(24), 5049–5055.
16 N. Leconte, D. Soriano, S. Roche, P. Ordejón, J. C. Charlier and J. J. Palacios, *ACS Nano*, 2011, **5**, 3987–3992.
17 X. Jiang, J. Nisar, B. Pathak, J. Zhao and R. Ahuja, *J. Catal.*, 2013, **299**, 204–209.
18 M. R. Rezapour, G. Lee and K. S. Kim, *Carbon*, 2019, **153**, 525–530.
19 I. Choudhuri, N. Patra, A. Mahata, R. Ahuja and B. Pathak, *J. Phys. Chem. C*, 2015, **119**, 24827–24836.
20 S. M. Avdoshenko, D. Nozaki, C. Gomes da Rocha, J. W. González, M. H. Lee, R. Gutierrez and G. Cuniberti, *Nano Lett.*, 2013, **13**, 1969–1976.
21 H. S. Kim and Y. H. Kim, *Biosens. Bioelectron.*, 2015, **69**, 186–198.
22 B. Biel, F. Triozon, X. Blase and S. Roche, *Nano Lett.*, 2009, **9**, 2725–2729.
23 M. R. Rezapour, G. Lee and K. S. Kim, *Nanoscale Adv.*, 2020, **2**, 5905–5911.
24 T. Ahmed, S. Kilina, T. Das, J. T. Haraldsen, J. J. Rehr and A. V. Balatsky, *Nano Lett.*, 2012, **12**, 927–931.
25 J. H. Lee, Y. K. Choi, H. J. Kim, R. H. Scheicher and J. H. Cho, *J. Phys. Chem. C*, 2013, **117**, 13435–13441.
26 Y. Kubota, K. Watanabe, O. Tsuda and T. Taniguchi, *Science*, 2007, **317**, 932–934.
27 L. Song, L. Ci, H. Lu, P. B. Sorokin, C. Jin, J. Ni, A. G. Kvashnin, D. G. Kvashnin, J. Lou, B. I. Yakobson and P. M. Ajayan, *Nano Lett.*, 2010, **10**, 3209–3215.
28 B. Aufray, A. Kara, Ś. Vizzini, H. Oughaddou, C. Ĺandri, B. Ealet and G. L. Lay, *Appl. Phys. Lett.*, 2010, **96**, 183102.
29 P. Vogt, P. De Padova, C. Quaresima, J. Avila, E. Frantzeskakis, M. C. Asensio, A. Resta, B. Ealet and G. L. Lay, *Phys. Rev. Lett.*, 2012, **108**, 155501.
30 M. E. Dávila, L. Xian, S. Cahangirov, A. Rubio and G. Le Lay, *New J. Phys.*, 2014, **16**, 095002.
31 F. Zhu, W. Chen, Y. Xu, C. Gao, D. Guan and C. Liu, *Nat. Mater.*, 2015, **14**, 1020–1025.
32 S. Das, M. Demarteau and A. Roelofs, *ACS Nano*, 2014, **8**, 11730–11738.

33 L. Li, Y. Yu, G. J. Ye, Q. Ge, X. Ou, H. Wu, D. Feng and X. H. Chen, *Nat. Nanotechnol.*, 2014, **9**, 372–377.
34 A. K. Geim and I. V. Grigorieva, *Nature*, 2013, **499**, 419–425.
35 Q. H. Wang, K. Kalantar-Zadeh, A. Kis, J. N. Coleman and M. S. Strano, *Nat. Nanotechnol.*, 2012, **7**, 699–712.
36 A. Molle, C. Grazianetti, L. Tao, D. Taneja, M. HasibulAlam and D. Akinwande, *Chem. Soc. Rev.*, 2018, **47**, 6370–6387.
37 L. Chen, C. C. Liu, B. Feng, X. He, P. Cheng, Z. Ding, S. Meng, Y. Yao and K. Wu, *Phys. Rev. Lett.*, 2012, **109**, 056804.
38 L. Tao, E. Cinquanta, D. Chiappe, C. Grazianetti, M. Fanciulli, M. Dubey, A. Molle and D. Akinwande, *Nat. Nanotechnol.*, 2015, **10**, 227–231.
39 M. E. Dávila and G. L. Lay, *Sci. Rep.*, 2016, **6**, 20714.
40 L. Zhang, P. Bampoulis, A. N. Rudenko, Q. Yao, A. van Houselt, B. Poelsema, M. I. Katsnelson and H. J. W. Zandvliet, *Phys. Rev. Lett.*, 2016, **116**, 256804.
41 A. Acun, L. Zhang, P. Bampoulis, M. Farmanbar, A. van Houselt, A. N. Rudenko, M. Lingenfelder, G. Brocks, B. Poelsema, M. I. Katsnelson and H. J. W. Zandvliet, *J. Phys.: Condens. Matter*, 2015, **27**, 443002.
42 S. Balendhran, S. Walia, H. Nili, S. Sriram and M. Bhaskaran, *Small*, 2015, **11**, 640–652.
43 E. Bianco, S. Butler, S. Jiang, O. D. Restrepo, W. Windl and J. E. Goldberger, *ACS Nano*, 2013, **7**, 4414–4421.
44 Q. Chen, L. Liang, G. Potsi, P. Wan, J. Lu, T. Giousis, E. Thomou, D. Gournis, P. Rudolf and J. Ye, *Nano Lett.*, 2019, **19**, 1520–1526.
45 Q. Pang, Y. Zhang, J. M. Zhang, V. Ji and K. W. Xu, *Nanoscale*, 2011, **3**, 4330–4338.
46 M. M. Monshi, S. M. Aghaei and I. Calizo, *RSC Adv.*, 2017, **7**, 18900.
47 A. Nijamudheen, R. Bhattacharjee, S. Choudhury and A. Datta, *J. Phys. Chem. C*, 2015, **119**, 3802–3809.
48 L. C. Loaiza, L. Monconduit and V. Seznec, *Small*, 2020, **16**, 1905260.
49 N. Liu, G. Bo, Y. Liu, X. Xu, Y. Du and S. X. Dou, *Small*, 2019, **15**, 1805147.
50 T. Hussain, T. Kaewmaraya, S. Chakraborty, H. Vovusha, V. Amornkitbamrung and R. Ahuja, *ACS Sens.*, 2018, **3**(4), 867–874.
51 J. Zhao, H. Liu, Z. Yu, R. Quhe, S. Zhou, Y. Wang, C. C. Liu, H. Zhong, N. Han, J. Lu, Y. Yao and K. Wu, *Prog. Mater. Sci.*, 2016, **83**, 24–151.
52 Q. Pang, L. Li, D. L. Gao, R. P. Chai, C. L. Zhang and Y. L. Song, *Phys. E*, 2017, **88**, 237–242.
53 J. Prasongkit, R. G. Amorim, S. Chakraborty, R. Ahuja, R. H. Scheicher and V. Amornkitbamrung, *J. Phys. Chem. C*, 2015, **119**, 16934–16940.
54 S. J. Heerema and C. Dekker, *Nat. Nanotechnol.*, 2016, **11**, 127–136.
55 M. M. Monshi, S. M. Aghaei and I. Clizo, *Surf. Sci.*, 2017, **665**, 96–102.
56 V. Nagarajan and R. Chandiramouli, *Superlattices Microstruct.*, 2017, **101**, 160–171.
57 V. Nagarajan and R. Chandiramouli, *J. Mol. Liq.*, 2017, **234**, 355–363.
58 R. G. Amorim and R. H. Scheicher, *Nanotechnology*, 2015, **26**, 154002.
59 T. Hussain, H. Vovusha, T. Kaewmaraya, V. Aamornkitbamrung and R. Ahuja, *Sens. Actuators, B*, 2018, **255**, 2713–2720.
60 A. C. Rajan, M. R. Rezapour, J. Yun, Y. Cho, W. J. Cho, S. K. Min, G. Lee and K. S. Kim, *ACS Nano*, 2014, **8**, 1827–1833.
61 A. E. Miroshnichenko, S. Flach and Y. S. Kivshar, *Rev. Mod. Phys.*, 2010, **82**, 2257.
62 G. Kresse and J. Furthmüller, *Phys. Rev. B: Condens. Matter Mater. Phys.*, 1996, **54**, 11169.
63 J. P. Perdew, K. Burke and M. Ernzerhof, *Phys. Rev. Lett.*, 1996, **77**, 3865–3868.
64 G. Kresse and D. Joubert, *Phys. Rev. B: Condens. Matter Mater. Phys.*, 1999, **59**, 1758.
65 S. D. Chakarova-Käck, E. Schröder, B. I. Lundqvist and D. C. Langreth, *Phys. Rev. Lett.*, 2006, **96**, 146107.
66 J. Björk, F. Hanke, C. A. Palma, P. Samori, M. Cecchini and M. Persson, *J. Phys. Chem. Lett.*, 2010, **1**, 3407–3412.
67 A. Tkatchenko and M. Scheffler, *Phys. Rev. Lett.*, 2009, **102**, 073005.
68 T. Bučko, S. Lebègue, J. Hafner and J. G. Ángyán, *Phys. Rev. B: Condens. Matter Mater. Phys.*, 2013, **87**, 064110.
69 J. Taylor, H. Guo and J. Wang, *Phys. Rev. B: Condens. Matter Mater. Phys.*, 2001, **63**, 245407.
70 S. Datta, *Electronic Transport in Mesoscopic Systems*, Cambridge University Press, Cambridge, 1997.
71 M. Brandbyge, J. L. Mozos, P. Ordejón, J. Taylor and K. Stokbro, *Phys. Rev. B: Condens. Matter Mater. Phys.*, 2002, **65**, 165401.
72 S. Cahangirov, M. Topsakal and S. Ciraci, *Phys. Rev. B: Condens. Matter Mater. Phys.*, 2010, **81**, 195120.
73 S. Cahangirov, M. Topsakal, E. Aktürk, H. Şahin and S. Ciraci, *Phys. Rev. Lett.*, 2009, **102**, 236804.
74 H. K. Gürel and B. Salmankurt, *Biosensors*, 2021, **11**, 59–72.
75 G. Liu, W. W. Luo, X. Wang, X. L. Lei, B. Xu, C. Y. Ouyang and S. B. Liu, *J. Mater. Chem. C*, 2018, **6**, 5937–5948.
76 I. S. S. de Oliveira and R. H. Miwa, *J. Chem. Phys.*, 2015, **142**, 044301.
77 S. S. Raya, A. S. Ansari and B. Shong, *Surf. Interfaces*, 2021, **24**, 101054.
78 S. Gowtham, R. H. Scheicher, R. Ahuja, R. Pandey and S. P. Karna, *Phys. Rev. B: Condens. Matter Mater. Phys.*, 2007, **76**, 033401.
79 M. R. Rezapour, A. C. Rajan and K. S. Kim, *J. Comput. Chem.*, 2014, **35**, 1916–1920.
80 W. Xia, W. Hu, Z. Li and J. Yang, *Phys. Chem. Chem. Phys.*, 2014, **16**, 22495–22498.